RESEARCH PAPER

Innovative Construction of SrTiO$_3$ Nanoparticle/ZnO Nanorod Heterojunction Photocatalyst for Hydrogen Production Under Simulated Sunlight Radiation

Ghader Hosseinzadeh

Department of Chemical Engineering, University of Bonab, Bonab, Iran

ARTICLE INFO

ABSTRACT

In the current study, an innovative hydrothermal method was proposed for synthesis of the 0D/1D heterojunction nanocomposite of SrTiO$_3$/ZnO from the combination of ZnO nanorod, SrTiO$_3$ nanoparticle, for the first time. The prepared nanocomposite was fully characterized by XRD, FESEM, DRS, PL, and Mott-Schottky analysis and was applied for the first time for photocatalytic Hydrogen production under simulated sunlight irradiation. The results revealed that, the heterojunction sample had better photocatalytic performance than pure SrTiO$_3$ and ZnO samples, and 25 mmol hydrogen molecule can be produced per gram of this heterojunction nanocomposite during 3 hours irradiation time. The enhanced photocatalytic activity of this heterojunction is attributed to the decreasing of the charge carrier's recombination rate, and enhanced visible light harvesting. Moreover, based on the results from experiments and Mott-Schottky calculations a type II charge transfer mechanism revealed to be responsible for the enhanced photocatalytic performance. In this mechanism, the photoinduced electrons on conduction band of SrTiO$_3$ nanoparticle migrate to the conduction band of ZnO nanorod, and the photoinduced holes on the valence band of ZnO nanorod migrate to the valence band SrTiO$_3$ nanoparticle, which results in the decreasing of the charge carrier's recombination rate.

INTRODUCTION

Nowadays, Because of the increasing global energy demand, there is a serious need for the development of new energy resources, however, considering of the environmental pollution issues, the clean and renewable energy sources is the best choice [1]. Among the clean and sustainable energy sources, Hydrogen energy recognized as a promising one because of its characteristics of less environmental pollution, convenient storage and high energy density [2, 3]. There are many methods for hydrogen production such as methane steam reforming (MSR) reaction, electrolysis of water, and gasification of coal, however, photocatalytic water splitting by semiconductor photocatalysts is cost-effective, highly efficient, clean and environmentally friendly technique [2, 4].

ZnO semiconductor has been extensively used for photocatalytic Hydrogen production from water splitting because of its excellent features such as environmental friendliness, good stability, non-toxicity, and low cost [5, 6]. However, ZnO

* *Corresponding Author Email: g.hosseinzadeh@ubonab.ac.ir*

has a poor photocatalytic Hydrogen production activity due to the low visible light absorption, and fast charge carriers recombination rate [7, 8]. In this regards, various strategies have been suggested for improvement of its photocatalytic performance, such as doping with other elements [9], compositing with carbon nanostructures [10, 11], surface engineering [12], and hybridization with other semiconductor photocatalysts in heterojunction nanocomposites [13-15]. Among these methods, construction of the heterojunction photocatalysts are promising one because it could efficiently separate photo-induced electron/hole pairs [16]. Different heterojunction nanocomposites of ZnO were synthesized such as Bi_2O_3/ZnO [12], ZnO/BiVO$_4$ [17], WO$_3$/ZnO [18], ZnO/ZnS [19], and ZnO/AgBr [20].

Strontium titanate (SrTiO$_3$) has a cubic perovskite structure of ABO$_3$, with Sr^{2+} and Ti^{4+} in the A and B sites, respectively [21]. This n-type semiconductor with band gap of ~3.2 eV has been widely used as an efficient photocatalyst in a wide range of photocatalytic applications due to its suitable valence and conduction band position, good structural and thermal stability, resistance to photo-corrosion and excellent photocatalytic activity [22, 23]. However, because of its high band gap and fast charge carriers recombination rate, this semiconductor has low photocatalytic efficiency under sunlight irradiation [24]. For improvement of its photocatalytic performance this semiconductor is used as a cocatalyst with other semiconductors in a heterojunction forms and different heterojunction nanocomposites of SrTiO$_3$ were synthesized such as WO$_3$/SrTiO$_3$ [25], g-C$_3$N$_4$/SrTiO$_3$ [26], SrTiO$_3$/Bi$_2$S$_3$ [27], and SrTiO$_3$/BiOBr [28].

Inspired from the above discussions, in current study, ZnO/SrTiO$_3$ heterojunction nanocomposite was synthesized from new method by compositing of ZnO nanorods, and SrTiO$_3$ nanoparticles through hydrothermal technique and was applied for photocatalytic Hydrogen production under simulated sunlight irradiation. Due to the many advantages of hydrothermal method such as high purity and homogeneity of product, narrow particles distribution, high yield, cost-effectiveness, and ease of morphology controlling [29], this technique was used for preparation of the nanocomposite. The as-prepared composite was fully characterized by XRD, FESEM, DRS, PL, and Mott-Schottky analysis. Furthermore,

based on the optical, photoelectrochemical and photocatalytic activity tests results, a possible charge transfer mechanism was proposed.

MATERIALS AND METHODS
Materials
Zn(NO$_3$)$_2$.6H$_2$O, 25% ammonia solution, Na$_2$CO$_3$, ethanol, ethylene glycol, Titanium butoxide, Sr(NO$_3$)$_2$ and KOH were purchased in analytical grade from Merck, Germany, and were used as raw materials without any purification.

Synthesis of ZnO nanorods
ZnO nanorods were prepared by hydrothermal method. Briefly, 5 mmol of Zn(NO$_3$)$_2$.6H$_2$O was dissolved in 50 ml ethylene glycol, the final solution was obtained by adding 3 ml of 25% ammonia solution and 5 mmol of Na$_2$CO$_3$. Then the resulted mixture was subjected to hydrothermal process in a 75 ml Teflon lined stainless autoclave and maintained at 120 ℃ for 10 hours. Preparation in nonaqueous solvent and presence of Na$_2$CO$_3$ may induce preferred growth in one direction and lead to the formation of nanorod morphology during the hydrothermal method [30]. The obtained ZnO nanorods was separated by centrifuging and washed several times with distilled water and ethanol and dried at 60 ℃.

Synthesis of SrTiO$_3$ nanoparticles
Hydrothermal technique was used for preparation of SrTiO$_3$ nanoparticles. For this purpose, 3.5 ml of Titanium butoxide was dissolved in 25 ml of Butanol then under magnetic stirring 2.1 g of Sr(NO$_3$)$_2$ was added, After addition of 25 ml of 2 M KOH solution, the final solution was transferred into a 75 ml Teflon lined stainless autoclave vessel and maintained at 200 °C for 12h. The final precipitates were immediately separated-out by centrifugation, washed several times with distilled water and ethanol, and dried at 60 °C.

Synthesis of ZnO/SrTiO$_3$ heterojunction nanocomposite
For synthesis of ZnO/SrTiO$_3$ heterojunction nanocomposite, containing 35% (w/w) ZnO and 65% (w/w) SrTiO$_3$, in a typical process, 1 g ZnO nanorods were fully dispersed in 25 ml of Butanol by probe ultrasonication, then 3.5 ml of Titanium butoxide and 2.1 g of Sr(NO$_3$)$_2$ were disolved in above suspension by magnetic stirring. After addition of 25 ml of 2 M KOH solution, the final

suspension was poured into a 75 ml Teflon lined stainless autoclave and maintained at 200 °C for 12h. The resulted nanocomposite were separated-out by centrifugation, washed several times with distilled water and ethanol, and dried at 60 °C.

Characterizations

The crystal characteristics of the obtained photocatalysts were analyzed by X-ray diffraction (XRD) on Philips X' Pert MPD with Cu Kα radiation (λ= 0.15406 nm) in 2θ range from 10° to 80°. MIRA3 TESCAN field emission scanning electron microscopy (FESEM) was applied to investigate the morphology and particle size of the photocatalyst samples. Diffuse reflectance spectroscopy (DRS) in the region of 200 to 800 nm was performed by means of a Shimadzu UV-2550 UV–vis spectrophotometer. Varian Cary-Eclipse 500 fluorescence spectrometer was used to obtain the photoluminescence (PL) spectra of samples at excitation wavelength of 300 nm. Photo-electrochemical characteristics of the samples were assessed using a Gamry potentiostat in a conventional three electrode system of Pt foil (counter electrode), Ag/AgCl (reference electrode),

and the prepared samples as working electrode under 570W Xenon lamp as the simulated sunlight source.

Photocatalytic activity

The photocatalytic H$_2$ production tests were conducted in a quartz reactor. In a typical process, 100 mg of the prepared photocatalyst samples were fully dispersed by ultrasonication in 100 ml deionized water containing TEOA as sacrificial agents, then this suspension was deoxygenated by nitrogen gas purging for 20 min. The resulted suspension was stirred under dark condition for 1 h to reach an adsorption–desorption equilibrium, and afterward was irradiated with a 570W Xenon lamp (as a simulated solar light source) at 25°C. The yield of hydrogen was measured by Shimadzu GC-2014 gas chromatograph by using N$_2$ gas as carrier gas with a TCD detector.

RESULTS AND DISCUSSION
XRD

The XRD patterns of the prepared samples were illustrated in Fig. 1. For ZnO sample, the main peaks of (100), (002), (101), (102), (110), (103),
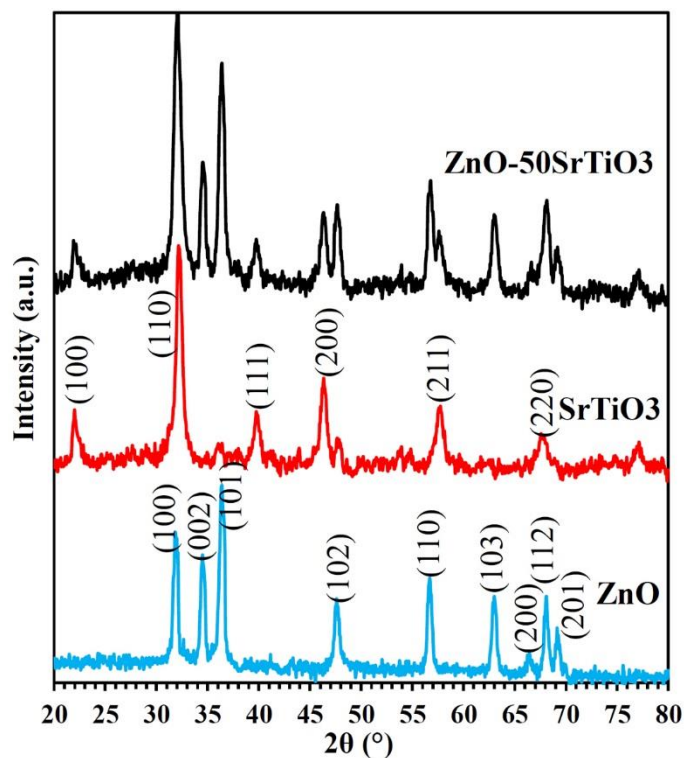
Fig. 1. XRD patterns of the prepared samples.
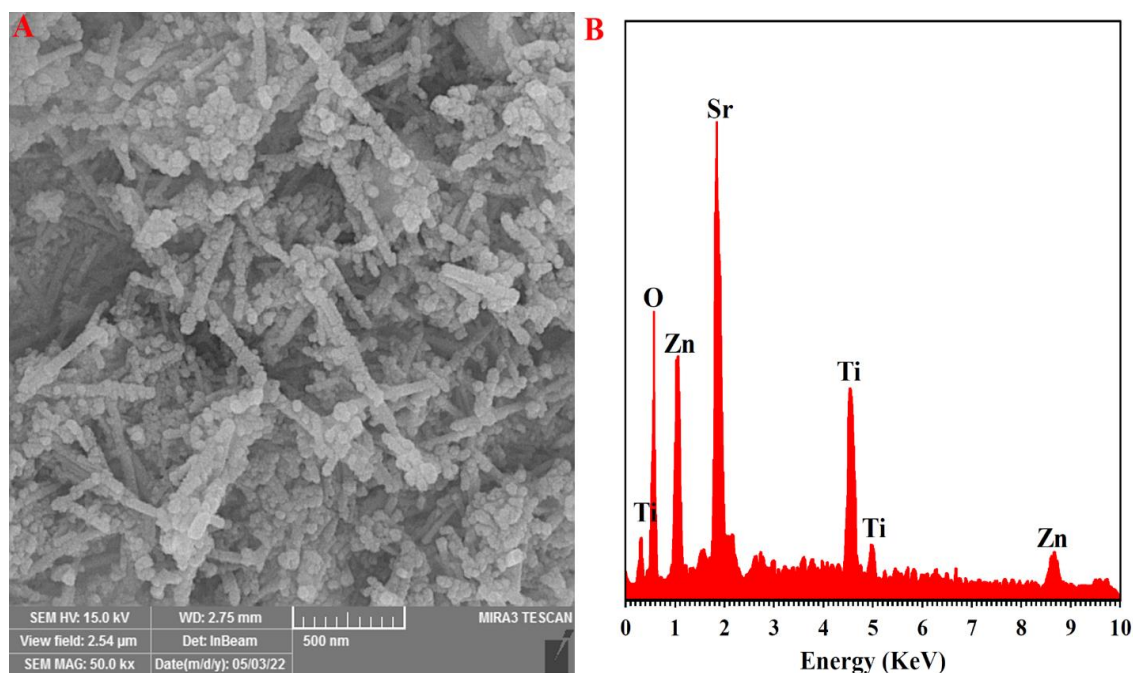
Fig. 2. FE-SEM image (A) and EDS spectrum (B) of ZnO/SrTiO₃ heterojunction nanocomposite.

(200), (112), and (201) are present at 2θ of 31.7º, 34.3º, 36.2º, 47.6 º, 56.4º, 62.9º, 66.3º, 67.9º, and 69.1º, respectively, which well matched with wurtzite structure of ZnO (JCPDS # 36-1451) [31]. In XRD pattern of SrTiO₃, the diffraction peaks positioned at 2θ of 22.2, 32.3, 39.9, 46.2, 57.6, and 67.7° can be indexed to the (100), (110), (111), (200), (211), and (220) diffraction planes of the cubic perovskite SrTiO₃ with JCPDS card no. 35–0734 [36]. In the diffraction patterns of ZnO/SrTiO₃ heterojunction sample, the characteristic diffraction peaks of both SrTiO₃ and ZnO are present, denoting that the nanocomposite sample are successfully synthesized. The broadening of the diffraction peaks indicates nanostructure nature of the prepared samples.

FE-SEM

The FE-SEM images were taken from the ZnO/SrTiO₃ sample to characterize its morphology and particle size. The results of FE-SEM images for this sample is given in Fig. 2 (A). As seen in this image, this sample contains the ZnO nanorods with an approximate diameter of 50 nm and an approximate length of 600 nm, and SrTiO₃ nanoparticles with size of about 30 nm. Furthermore, the well distribution of the SrTiO₃ nanoparticles on the ZnO nanorods is clearly

observed in this image.

To verify the presence of SrTiO₃ and ZnO compounds in the ZnO/SrTiO₃ heterojunction nanocomposite, EDS analysis were carried out on this sample. Fig. 2 (B) shows the EDS spectrum of the ZnO/SrTiO₃ sample. In the EDS spectrum, peaks corresponding to Ti, Sr, O and Zn can be obviously observed, suggesting the coexistence of SrTiO3 and ZnO in the ZnO/SrTiO₃ sample, which demonstrates successfully synthesis of the ZnO/SrTiO₃ heterojunction nanocomposite.

DRS

In order to evaluate the photocatalytic performance of a photocatalyst, its optical behavior must be examined. To study the photo-response characteristics of the prepared samples, the light absorption spectra of the prepared samples were tested by UV-Vis diffuse reflectance spectroscopy (UV-DRS), and the relevant results are shown in Fig. 3. As it is clearly seen in Fig. 3(A), the absorption edges of the SrTiO₃, ZnO, and ZnO/SrTiO₃ samples are found to be around 380, 410, and 410 nm, respectively. As can be seen, SrTiO₃ nanoparticles mainly absorb the ultraviolet light. The presence of ZnO in the structure of SrTiO₃ shifts the SrTiO₃ absorption edge towards the visible light region, which can improve the photocatalytic
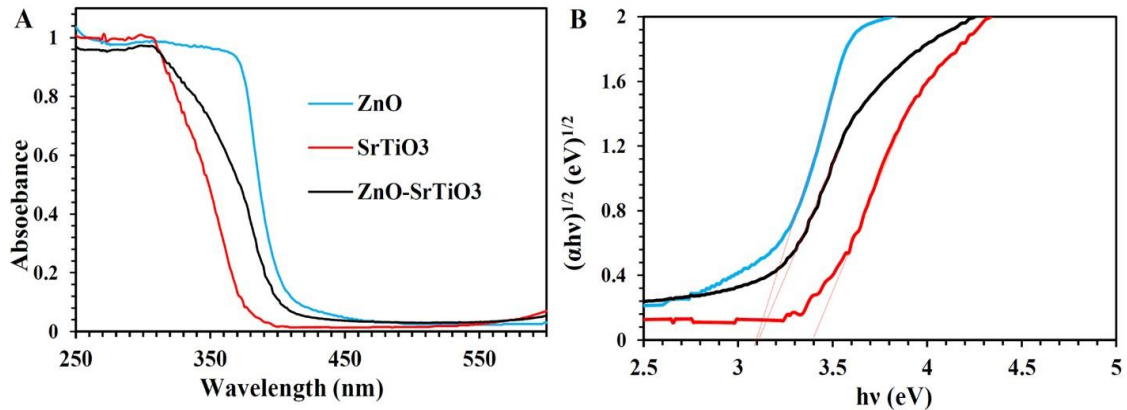
Fig. 3. (a) UV-Vis diffuse reflectance and (b) Tauc plots for the corresponding samples.

performance of the nanocomposite sample under solar light radiation. In order to study this effect more precisely, the band gap energy of the samples was examined based on Tauc formula [32]. As shown in (Fig. 3(B)) the band gap energies of the $SrTiO_3$, ZnO, and $ZnO/SrTiO_3$ samples are 3.4, 3.1, and 3.1 eV, respectively. Therefore heterojunction formation between $SrTiO_3$ and ZnO, remarkably decreases the band gap energy of $SrTiO_3$, which could results in an improvement of photocatalytic activity under solar light irradiation.

Photoluminescence (PL)

The separation of charge carriers, i.e. photoinduced electrons and holes, is one of the effective factors on the photocatalytic performance of a photocatalyst sample (PL) spectroscopy can be used to study the effect heterojunction formation between ZnO and $SrTiO_3$ semiconductors on the separation and transportation of charge carriers in the $ZnO/SrTiO_3$ heterojunction sample. In this case, any decrease in the PL intensity indicates a decrease in the electron-hole recombination
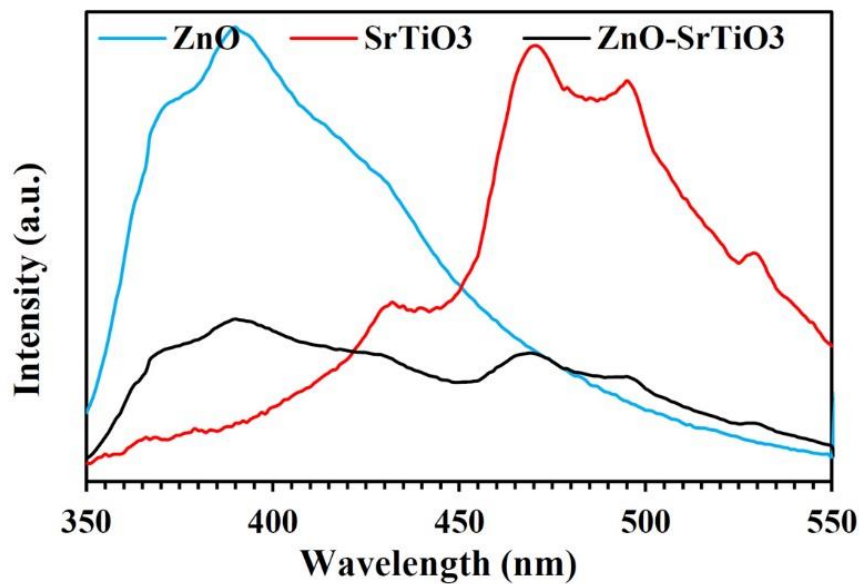
Fig. 4. PL spectra of the prepared samples.
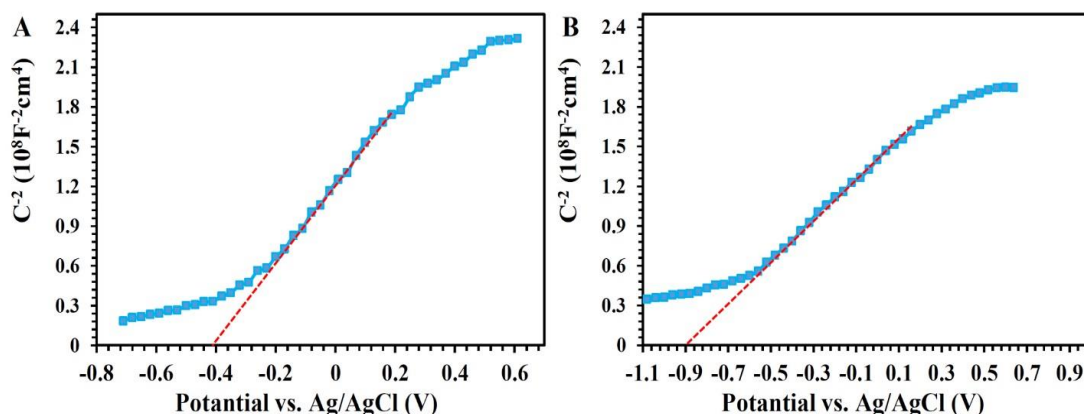
Fig. 5. Mott-Schottky measurements for (A) ZnO and (B) SrTiO$_3$ samples.

which can results in the improvement of the photocatalyst performance [33]. As can be seen in Fig. 4, the PL intensity of the ZnO/SrTiO$_3$ nanocomposite is remarkably lower than that of the SrTiO$_3$ and ZnO samples, so it can be concluded that heterojunction formation between ZnO and SrTiO$_3$ effectively reduced the electron-hole recombination. Therefore, the ZnO/SrTiO$_3$ sample could has the improved photocatalytic activity due to the diminished charge carriers recombination rate.

Mott-Schottky

To determine the conduction and valance band energies of the ZnO and SrTiO$_3$ samples, Mott-Schottky tests were conducted, as depicted in (Fig. 5). The Mott-Schottky curves of ZnO and SrTiO$_3$ samples have positive slopes, reflecting that these samples are n-type semiconductors [34]. The flat band potentials (E$_{FB}$) for pure ZnO and SrTiO$_3$ were found to be -0.4 and -0.9 V versus Ag/AgCl reference electrode (-0.2 and -0.7 V relative to NHE), respectively. It is generally documented
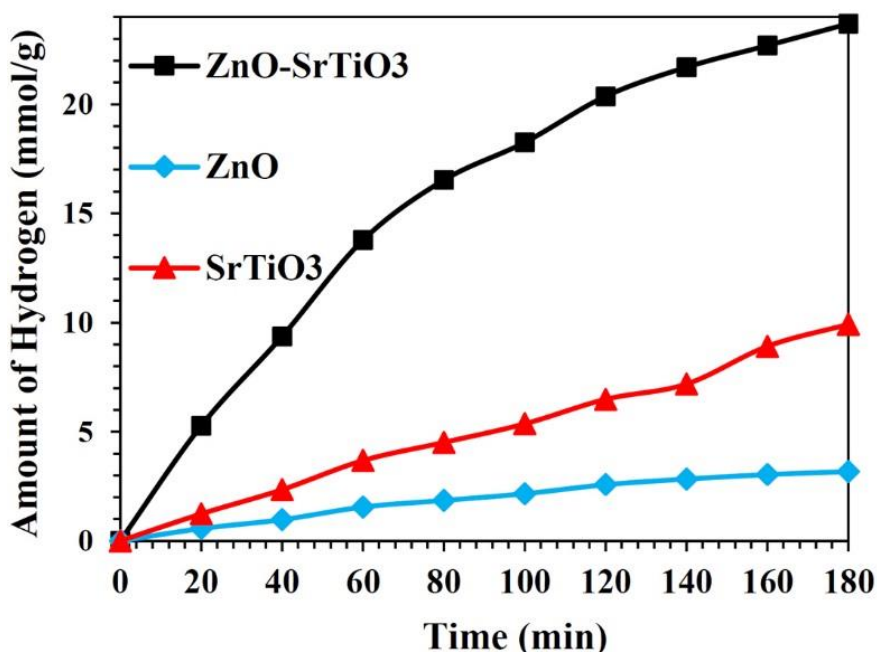
Fig. 6. Simulated sunlight photocatalytic hydrogen production over the prepared samples.
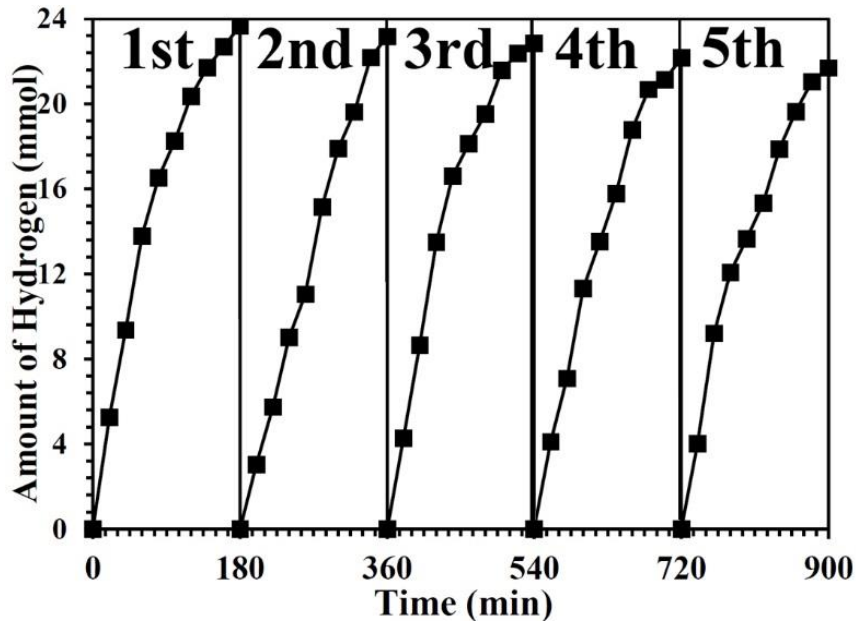
Fig. 7. Cycles for the photocatalytic Hydrogen production performance of the ZnO/SrTiO₃ heterojunction under simulated sunlight irradiation.

that the conduction band potential (E_C) in n-type semiconductors is located ~0.1 eV lower than E_{FB}, and the potential of valance band (E_V) of p-type semiconductors is approximately 0.1 V higher than E_{FB} [35]. In this regard, E_C of ZnO and SrTiO₃ samples are calculated around -0.3 and -0.8 eV vs.
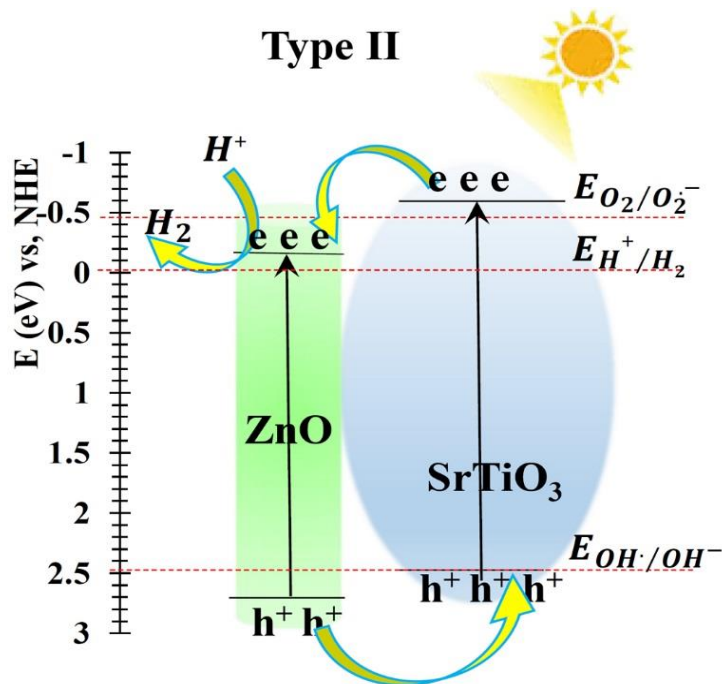
Fig. 8. Plausible type II charge transfer pathways for the photocatalytic Hydrogen production on the ZnO/SrTiO₃ heterojunction under simulated sunlight irradiation.

NHE, respectively. Further, E$_V$ of ZnO and SrTiO$_3$ samples are estimated through the equation E$_V$=E$_g$ + E$_C$, therefore E$_V$ of these samples are 2.8 and 2.6 eV vs. NHE, respectively.

Photocatalytic performance

The photocatalytic efficiencies of the prepared photocatalyst samples were examined by measuring the photocatalytic hydrogen production under simulated sunlight irradiation. As shown in Fig. 6. The photocatalytic performance of the ZnO/SrTiO$_3$ heterojunction nanocomposite photocatalyst is about 10 times and three time higher than that of the pure ZnO and SrTiO$_3$ samples, respectively, and the ZnO/SrTiO$_3$ nanocomposite could produce 25 mmol hydrogen molecule during 3 hours simulated sunlight irradiation. The significantly improved photocatalytic performance of the ZnO/SrTiO$_3$ sample can be attributed to the decreasing of the charge carriers recombination rate and improvement of the visible light absorbance harvesting.

For investigation the stability of the ZnO/SrTiO$_3$ heterojunction nanocomposite during the hydrogen production reaction condition, recycling test was done on this sample. As shown in Fig. 7, the ZnO/SrTiO$_3$ sample has reasonable stability during the photocatalytic hydrogen production reaction and maintains 92% of its initial activity after five successive cycles. Therefore this heterojunction could be recycled and reused many times for photocatalytic hydrogen evolution without significant reduction in its activity.

Plausible type II charge transfer pathways for the photocatalytic Hydrogen production activity of the ZnO/SrTiO$_3$ heterojunction are thoroughly discussed in Fig.8. In type II mechanism, during the simulated sunlight irradiation of the heterojunction photocatalyst, the electrons on conduction band of SrTiO$_3$ nanoparticles migrate to the conduction band of ZnO nanorods, on the other hand, the photoinduced holes on the valence band of ZnO nanorods migrate to the valence band SrTiO$_3$ nanoparticles [11]. In this regard, the charge carriers are efficiently separated, which results in the production of more photoinduced electrons for reduction of H$^+$ to H$_2$.

CONCLUSION

In summary, a novel ZnO nanorod/SrTiO$_3$ nanoparticles heterojunction photocatalyst was synthesized from the combination of ZnO nanorod and SrTiO$_3$ nanoparticles through innovative hydrothermal technique and was applied for first time for photocatalytic hydrogen production under simulated sunlight irradiation. According to the obtained results, the highest photocatalytic efficiency was obtained for the ZnO/SrTiO$_3$ heterojunction sample which is attributed to the decreasing of the charge carriers recombination rate, and enhanced visible light harvesting. Moreover, based on the Mott-Schottky calculations, a type II charge transfer pathway was suggested for the enhancement of the photocatalytic performance on the prepared heterojunction nanocomposite.

CONFLICT OF INTEREST

The authors declare that there is no conflict of interests regarding the publication of this manuscript.

REFERENCES

1. Chaurasia AK, Mohapatra S, Shankar R, Thakur LS. Technologies for the Clean and Renewable Energy Production for the Sustainable Environment. Advances in Civil and Industrial Engineering: IGI Global; 2022. p. 141-178.
2. Shangguan W, Kudo A, Jiang Z, Yamaguchi Y. Photocatalysis: from solar light to hydrogen energy. Frontiers in Energy. 2021;15(3):565-567.
3. Yue M, Lambert H, Pahon E, Roche R, Jemei S, Hissel D. Hydrogen energy systems: A critical review of technologies, applications, trends and challenges. Renewable and Sustainable Energy Reviews. 2021;146:111180.
4. Yang Y, Zhou C, Wang W, Xiong W, Zeng G, Huang D, et al. Recent advances in application of transition metal phosphides for photocatalytic hydrogen production. Chem Eng J. 2021;405:126547.
5. Dhiman P, Rana G, Kumar A, Sharma G, Vo D-VN, Naushad M. ZnO-based heterostructures as photocatalysts for hydrogen generation and depollution: a review. Environ Chem Lett. 2022;20(2):1047-1081.
6. Kumar S, Kumar A, Kumar A, Krishnan V. Nanoscale zinc oxide based heterojunctions as visible light active photocatalysts for hydrogen energy and environmental remediation. CarRv. 2019;62(3):346-405.
7. Bahadoran A, Masudy-Panah S, De Lile JR, Li J, Gu J, Sadeghi B, et al. Novel 0D/1D ZnBi$_2$O$_4$/ZnO S-scheme photocatalyst for hydrogen production and BPA removal. International Journal of Hydrogen Energy. 2021;46(47):24094-24106.
8. Habibi-Yangjeh A, Pirhashemi M, Ghosh S. ZnO/ZnBi2O4 nanocomposites with p-n heterojunction as durable visible-light-activated photocatalysts for efficient removal of organic pollutants. Journal of Alloys and Compounds. 2020;826:154229.
9. Liang S, Sui G, Li J, Guo D, Luo Z, Xu R, et al. ZIF-L-derived porous C-doped ZnO/CdS graded nanorods with Z-scheme heterojunctions for enhanced photocatalytic hydrogen evolution. International Journal of Hydrogen Energy.

2022;47(21):11190-11202.

10. Wang J, Wang G, Jiang J, Wan Z, Su Y, Tang H. Insight into charge carrier separation and solar-light utilization: rGO decorated 3D ZnO hollow microspheres for enhanced photocatalytic hydrogen evolution. Journal of Colloid and Interface Science. 2020;564:322-332.

11. Kim D, Yong K. Boron doping induced charge transfer switching of a C_3N_4/ZnO photocatalyst from Z-scheme to type II to enhance photocatalytic hydrogen production. Applied Catalysis B: Environmental. 2021;282:119538.

12. Wang X, Xu H, Zhang Y, Ji X, Zhang R. Fructose-regulated ZnO single-crystal nanosheets with oxygen vacancies for photodegradation of high concentration pollutants and photocatalytic hydrogen evolution. Ceram Int. 2021;47(11):16170-16177.

13. Ramírez-Ortega D, Guerrero-Araque D, Acevedo-Peña P, Reguera E, Calderon HA, Zanella R. Enhancing the photocatalytic hydrogen production of the ZnO–TiO2 heterojunction by supporting nanoscale Au islands. International Journal of Hydrogen Energy. 2021;46(69):34333-34343.

14. Jia Y, Wang Z, Qiao X-Q, Huang L, Gan S, Hou D, et al. A synergistic effect between S-scheme heterojunction and Noble-metal free cocatalyst to promote the hydrogen evolution of ZnO/CdS/MoS2 photocatalyst. Chem Eng J. 2021;424:130368.

15. Park BH, Park H, Kim T, Yoon SJ, Kim Y, Son N, et al. S-scheme assisted Cu_2O/ZnO flower-shaped heterojunction catalyst for breakthrough hydrogen evolution by water splitting. International Journal of Hydrogen Energy. 2021;46(77):38319-38335.

16. Raja VR, Muthupandi K, Nithya L. Facile synthesis of heterogeneous CdO-NiO nanocomposite with efficient photocatalytic activity under visible light irradiation. Environmental Chemistry and Ecotoxicology. 2021;3:76-84.

17. Li J, Yuan H, Li J, Zhang W, Liu Y, Liu N, et al. The significant role of the chemically bonded interfaces in $BiVO_4$/ZnO heterostructures for photoelectrochemical water splitting. Applied Catalysis B: Environmental. 2021;285:119833.

18. He L, Zhang S, Zhang J, Chen G, Meng S, Fan Y, et al. Investigation on the Mechanism and Inner Impetus of Photogenerated Charge Transfer in WO_3/ZnO Heterojunction Photocatalysts. The Journal of Physical Chemistry C. 2020;124(51):27916-27929.

19. Ren Z, Li X, Guo L, Wu J, Li Y, Liu W, et al. Facile synthesis of ZnO/ZnS heterojunction nanoarrays for enhanced piezo-photocatalytic performance. Materials Letters. 2021;292:129635.

20. Buapoon S, Phuruangrat A, Thongtem T, Thongtem S. AgBr nanoparticles–ZnO flowers nanocomposites used for photodegradation of methylene blue solution illuminated by ultraviolet-visible radiation. Inorganic and Nano-Metal Chemistry. 2020;51(4):523-530.

21. Miyauchi M, Takashio M, Tobimatsu H. Photocatalytic Activity of SrTiO₃ Codoped with Nitrogen and Lanthanum under Visible Light Illumination. Langmuir. 2003;20(1):232-236.

22. Jiang J, Kato K, Fujimori H, Yamakata A, Sakata Y. Investigation on the highly active SrTiO₃ photocatalyst toward overall H_2O splitting by doping Na ion. Journal of

Catalysis. 2020;390:81-89.

23. Cakra Wardhana A, Yamaguchi A, Shoji S, Liu M, Fujita T, Hitosugi T, et al. Visible-light-driven photocatalysis via reductant-to-band charge transfer in Cr(III) nanocluster-loaded SrTiO₃ system. Applied Catalysis B: Environmental. 2020;270:118883.

24. Kumar A, Sharma SK, Kumar A, Sharma G, AlMasoud N, Alomar TS, et al. High interfacial charge carrier separation in Fe_3O_4 modified SrTiO₃/$Bi_4O_5I_2$ robust magnetic nano-heterojunction for rapid photodegradation of diclofenac under simulated solar-light. Journal of Cleaner Production. 2021;315:128137.

25. Wu Y, Wei Y, Guo Q, Xu H, Gu L, Huang F, et al. Solvothermal fabrication of La-WO₃/SrTiO₃ heterojunction with high photocatalytic performance under visible light irradiation. Sol Energy Mater Sol Cells. 2018;176:230-238.

26. Konstas P-S, Konstantinou I, Petrakis D, Albanis T. Synthesis, Characterization of g-C_3N_4/SrTiO₃ Heterojunctions and Photocatalytic Activity for Organic Pollutants Degradation. Catalysts. 2018;8(11):554.

27. Ganapathy M, Hsu Y, Thomas J, Chen L-Y, Chang C-T, Alagan V. Preparation of SrTiO₃/Bi_2S_3 Heterojunction for Efficient Photocatalytic Hydrogen Production. Energy & Fuels. 2021;35(18):14995-15004.

28. Olagunju MO, Zahran EM, Zeynaloo E, Shukla D, Cohn JL, Surnar B, et al. Design of Pd-Decorated SrTiO₃/BiOBr Heterojunction Materials for Enhanced Visible-Light-Based Photocatalytic Reactivity. Langmuir. 2021;37(41):11986-11995.

29. H. Aboud K, Jamal Imran N, Al-Jawad SMH. Structural, Optical and Morphological Properties Cadmium Sulfide Thin Films Prepared by Hydrothermal Method. Journal of Applied Sciences and Nanotechnology. 2021;1(2):49-57.

30. Khoza PB, Moloto MJ, Sikhwivhilu LM. The Effect of Solvents, Acetone, Water, and Ethanol, on the Morphological and Optical Properties of ZnO Nanoparticles Prepared by Microwave. Journal of Nanotechnology. 2012;2012:1-6.

31. Sujinnapram S, Wongrerkdee S. Synergistic effects of structural, crystalline, and chemical defects on the photocatalytic performance of Y-doped ZnO for carbaryl degradation. JEnvS. 2023;124:667-677.

32. Lin Y, Wu S, Li X, Wu X, Yang C, Zeng G, et al. Microstructure and performance of Z-scheme photocatalyst of silver phosphate modified by MWCNTs and Cr-doped SrTiO₃ for malachite green degradation. Applied Catalysis B: Environmental. 2018;227:557-570.

33. Radha E, Komaraiah D, Sayanna R, Sivakumar J. Photoluminescence and photocatalytic activity of rare earth ions doped anatase TiO₂ thin films. Journal of Luminescence. 2022;244:118727.

34. Son N, Lee J, Yoon T, Kang M. Design for a longer photoinduced charge separation and improved visible-light-driven H_2 generation through structure reversal and oxygen vacancies via Ni substitution into $ZnFe_2O_4$ spinel. Ceram Int. 2021;47(14):20317-20334.

35. Das S, Patnaik S, Parida K. Dynamic charge transfer through Fermi level equilibration in the p-$CuFe_2O_4$/n-NiAl LDH interface towards photocatalytic application. Catalysis Science & Technology. 2020;10(18):6285-6298.